Mechanism of FAD Reduction and Role of Active Site Residues His-225 and Tyr-259 in *Arthrobacter globiformis* Dimethylglycine Oxidase: Analysis of Mutant Structure and Catalytic Function

Jaswir Basran,[‡] Stephen Fullerton,[‡] David Leys,[§] and Nigel S. Scrutton*[,§]

Department of Biochemistry, University of Leicester, Leicester LE1 9HN, U.K., and Faculty of Life Sciences and Manchester Interdisciplinary Biocentre, Jackson's Mill, Sackville Street, Manchester M60 1QD, U.K.

Received June 1, 2006; Revised Manuscript Received July 11, 2006

ABSTRACT: Residues His-225 and Tyr-259 are located close to the FAD in the dehydrogenase active site of the bifunctional dimethylglycine oxidase (DMGO) of *Arthrobacter globiformis*. We have suggested [Leys, D., Basran, J., and Scrutton, N. S. (2003) *EMBO J. 22*, 4038−4048] that these residues are involved in abstraction of a proton from the substrate amine group of dimethylglycine prior to C−H bond breakage and FAD reduction. To investigate this proposal, we have isolated two mutant forms of DMGO in which (i) His-225 is replaced with Gln-225 (H225Q mutant) and (ii) Tyr-259 is replaced with Phe-259 (Y259F mutant). Both mutant enzymes retain the ability to oxidize substrate, but the steady-state turnover of the Y259F mutant is attenuated more than 200-fold. Only modest changes in kinetic parameters are observed for the H225Q mutant during steady-state turnover. Stopped-flow studies indicate that the rate of FAD reduction in the Y259F enzyme is substantially impaired by a factor of ∼1500 compared with that of the wild-type enzyme, suggesting a key role for this residue in the reductive half-reaction of the enzyme. The kinetics of FAD reduction in the H225Q enzyme are complex and involve three discrete kinetic phases that are attributed to different conformational states of this mutant, evidence for which is provided by crystallographic analysis. Neither the H225Q enzyme nor the Y259F enzyme stabilizes the $FADH_2$−iminium charge-transfer complex observed previously in stopped-flow studies with the wild-type enzyme. Our studies are consistent with a key role for Tyr-259, but not His-225, in deprotonation of the substrate amine group prior to FAD reduction. We infer that residue His-225 is likely to modulate the acid−base properties of Tyr-259 by perturbing the pK_a of Tyr-259 and thus fine-tunes the reaction chemistry to facilitate proton abstraction under physiological conditions. Our data are discussed in the context of the crystallographic data for DMGO and also in relation to contemporary mechanisms for flavoprotein-catalyzed oxidation of amine substrates.

Dimethylglycine oxidase (DMGO)[1] (*1*) is a bifunctional flavoprotein isolated from *Arthrobacter globiformis* that catalyzes the oxidation of *N*,*N*-dimethylglycine and the formation of 5,10-methylene tetrahydrofolate. The enzyme is tetrameric with each monomer comprising two functionally distinct regions, as suggested from analysis of the protein sequence and structure (*1*, *2*). The N-terminal region (residues 1−420) binds FAD covalently and is responsible for the oxidation of dimethylglycine:

$$(CH_3)_2NCH_2COOH + O_2 + H_2O \rightarrow (CH_3)NHCH_2COOH + HCHO + H_2O_2$$

There are strong structural similarities between the N-terminal region of DMGO and monomeric sarcosine oxidase (*3*), polyamine oxidase (*4*), and *p*-hydroxybenzoate hydroxylase (*5*). The C-terminal region (residues 421−830) contains the second active site responsible for the formation of 5,10-methylene THF and comprises three domains arranged in a ringlike structure. This region of DMGO is related structurally to the T-protein of the glycine cleavage system (*6*), the ygfZ protein of *Escherichia coli* (*7*), and guanine nucleotide binding protein TrmE from *Thermotoga maritima* (*8*), suggesting that the THF-binding fold represented by the C-terminal DMGO region is widespread among folate-binding proteins (*9*). The crystal structure of DMGO indicates that the two active sites are ∼40 Å apart, connected by a large irregular internal cavity (*2*). The tetrahydrofolate-binding funnel located in the methylene transferase site (active site 2) serves as a transient entry−exit port, and access to the internal cavity is controlled kinetically by THF binding. It has been suggested that the internal cavity enables sequestration of the reactive iminium intermediate prior to reaction with tetrahydrofolate and prevents formation of toxic formaldehyde (*2*).

Detailed kinetic studies of FAD reduction and oxidation in DMGO by dimethylglycine and dioxygen, respectively, have been reported using stopped-flow methods (*10*). These studies have established a minimal kinetic mechanism

* To whom correspondence should be addressed. Telephone: +44 161 306 5152. Fax: +44 161 306 8918. E-mail: nigel.scrutton@manchester.ac.uk.

‡ University of Leicester.

§ Faculty of Life Sciences and Manchester Interdisciplinary Biocentre.

[1] Abbreviations: DMGO, dimethylglycine oxidase; THF, tetrahydrofolate.

10.1021/bi061094d CCC: $33.50
Published on Web 08/24/2006

Scheme 1

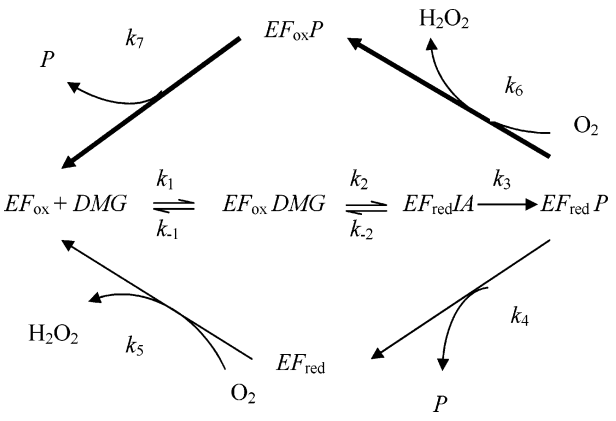

(Scheme 1) and provided spectroscopic evidence of the formation of a reduced flavin−iminium charge-transfer intermediate, $EF_{red}IA$, in the reductive half-reaction, similar to the "purple" intermediate identified in reactions with D-amino acid oxidase (*11*−*13*), tyramine oxidase (*14*), and L-phenylalanine oxidase (*15*). Decay of the enzyme−iminium charge-transfer intermediate is rate-limiting in steady-state reactions catalyzed by wild-type DMGO (*10*).

Despite intensive research efforts over a number of years, the mechanism of amine oxidation by flavoprotein enzymes remains contentious (*16*). Mechanisms involving (i) proton abstraction by an active site base to generate a carbanion species (*17*), (ii) an aminium radical cation species (*18*, *19*), (iii) H-atom abstraction by an active site radical species (*20*), and (iv) nucleophilic attack by the substrate nitrogen on the flavin C4a atom, followed by proton abstraction by an active site base (*21*) or the flavin N5 atom (*22*), have been considered over the years. On the basis of the crystal structure of wild-type DMGO, we have presented a hypothetical mechanism for FAD reduction that invoked a role for residues His-225 and Tyr-259 [highly conserved in the family of enzymes belonging to the sarcosine dehydrogenase class (*2*)] in facilitating deprotonation of the protonated amine substrate. This generates the free base form of the amine which was thought to form a covalent adduct at the FAD C4a position in a mechanism that is similar to that proposed previously for monoamine oxidase (*22*) and trimethylamine dehydrogenase (*23*). In this paper, we have addressed the role of these two residues in the catalytic mechanism. We have isolated two mutant forms of DMGO in which His-225 is exchanged for Gln-225 (H225Q) and Tyr-259 is exchanged for Phe-259 (Y259F). The properties and structures of the mutant enzymes suggest that neither residue is involved in deprotonating the substrate cation. Kinetic studies reveal that both mutant enzymes are active but that the Y259F enzyme is severely compromised in activity. Possible chemical mechanisms for the oxidation of dimethylglycine by DMGO are advanced that are consistent with both the reported kinetic and structural data.

EXPERIMENTAL PROCEDURES

Materials. Dimethylglycine, horseradish peroxidase, *o*-dianisidine, D-glucose, and glucose oxidase were purchased from Sigma-Aldrich Co. Restriction enzymes and DNA-modifying enzymes were from MBI fermentas. *Pfu Turbo* DNA polymerase and the QuikChange XL site-directed mutagenesis kit were from Stratagene. JM109 cells were obtained from Promega. dNTPs were from Amersham Pharmacia. Deuterated dimethylglycine was from CK Gas Products Ltd. Oligonucleotides were synthesized by the Protein and Nucleic Acid Chemistry Laboratory (University of Leicester). *N*,*N*-Dimethyl-d_6-glycine HCl was from CDN Isotopes (Quebec City, PQ).

DNA Manipulations. The pEH1 plasmid which harbors the *A. globiformis* gene encoding DMGO was used for expression of recombinant wild-type and mutant enzymes in *E. coli* (*10*). Plasmid pEH1 is large and unsuitable for routine mutagenesis. To facilitate the isolation of mutant forms of DMGO, the *dmg* gene encoding DMGO was amplified from pEH1 using *Pfu Turbo* DNA polymerase in a polymerase chain reaction (PCR) and cloned into pUC18. The primers 5′ CCT AAA TCT GCA GGA GAA TTC CAT GGC ATC GAC GCC G 3′ (forward primer) and 5′ CTC CCG TTG CGA GGA TAA GCT TGG CTG CGT GTC CCC G 3′ (reverse primer) were designed using the published *dmg* sequence (*1*) and used to clone *dmg* as an *Eco*RI and *Hin*dIII fragment into pUC18, producing the pUCDMGO plasmid. The *dmg* gene in this construct was resequenced to ensure that spurious changes had not arisen during the amplification procedure. Plasmid pUCDMGO was used as template DNA in all subsequent mutagenesis reactions. The H225Q and Y259F mutant DMGO enzymes were made using the QuikChange XL site-directed mutagenesis kit (Stratagene) and the oligonucleotides 5′ CCT GCT CCC GCT GGC CCA GCA GTA CGT AAA AAC CAC CCC 3′ and 5′ GGG GTG GTT TTT ACG TAC TGC TGG GCC AGC GGG AGC AGG 3′ for H225Q DMGO and 5′ CAC CAG GAC CAG GAC CTC TTT TAC CGC GAA CAC GGG GAC 3′ and 5′ GTC CCC GTG TTC GCG GTA AAA GAG GTC CTG GTC CTG GTG 3′ for Y259F DMGO. To ensure that no spurious changes had arisen as a result of the mutagenesis reactions, the entire *dmg* gene in each mutant construct was resequenced. To express high levels of each mutant protein in *E. coli*, the mutated DNA fragments were reintroduced into plasmid pEH1. This was achieved by digesting the mutant form of plasmid pUCDMGO with *Bsp*1407I and *Eco*RV restriction enzymes. The released *dmg*-containing fragment was used to replace the corresponding wild-type fragment in plasmid pEH1 which had previously been digested with *Bsp*1407I and *Eco*RV. The two mutant constructs were designated H225QpEH1 and Y259FpEH1, respectively.

Enzyme Expression and Purification. Recombinant wild-type and mutant forms of DMGO were expressed and purified from *E. coli* strain JM109 as described previously (*10*). The enzyme concentration was calculated using a molar extinction coefficient for the oxidized enzyme ($\epsilon_{444} = 12\,700$ M^{-1} cm^{-1}).

Preparation of Anaerobic Samples. Buffers were made anaerobic by bubbling argon gas through solutions for ~2 h. Solutions were then placed in an anaerobic glovebox (Belle Technology) overnight to remove any residual traces of oxygen. Samples of DMGO were made anaerobic by passing them through a small gel filtration (Bio-Rad 10 DG) column housed in the glovebox, which had been pre-equilibrated with anaerobic buffer. Solutions of dithionite and substrate were made by adding the appropriate solid to anaerobic buffer.

Kinetic Measurements. Steady-state kinetic parameters for DMGO activity (k_{cat} and K_m values) were obtained using the enzyme-monitored turnover method as described by Gibson et al. for reactions catalyzed by glucose oxidase (*24*). Reactions were performed at 25 °C in 10 mM sodium pyrophosphate buffer (pH 8.5) using an Applied Photophysics SX18-MV reaction analyzer. Data analysis was essentially as described previously (*24*). The oxygen concentration was varied by appropriate mixing of air-saturated buffer with anaerobic buffer prior to introduction into the stopped-flow instrument. The DMGO catalytic activity was also measured using a coupled enzyme assay in which the production of hydrogen peroxide was monitored using the reporter enzyme horseradish peroxidase (*1*). Assays were performed in a Hewlett-Packard 8452A spectrophotometer with a 1 cm light path.

Stopped-flow experiments of reductive and oxidative half-reactions were performed using an Applied Photophysics SX.18 MV stopped-flow spectrophotometer. The protein reaction cell concentration was 4 μM (for both reductive and oxidative half-reactions) for single-wavelength experiments and 10 μM for photodiode array experiments. All reactions were performed under anaerobic conditions achieved by housing the sample-handling unit of the stopped-flow instrument within an anaerobic glovebox (Belle Technology Ltd.). Unless otherwise stated, measurements were carried out at 25 °C in 10 mM sodium pyrophosphate buffer (pH 8.5). Due to the observed slow rate constants for flavin reduction in the mutant enzymes, the kinetics of the reductive half-reaction were analyzed in the presence of an oxygen scavenging system (glucose oxidase) to remove any residual traces of molecular oxygen which may complicate the analysis. Reactions were performed in the presence of 20 μg/mL glucose oxidase and 11 mM glucose (reaction cell concentrations).

Stopped-flow, multiple-wavelength absorption studies were carried out using a photodiode array detector and X-SCAN (Applied Photophysics Ltd.). Spectral deconvolution was performed by global analysis and numerical integration methods using PROKIN (Applied Photophysics Ltd.). In single-wavelength studies, flavin reduction by substrate was observed at 444 nm. For H225Q DMGO, transients were triphasic and were fitted using the standard triple-exponential expression (eq 1)

$$A_{444} = C_1 e^{-k_{obs1}t} + C_2 e^{-k_{obs2}t} + C_3 e^{-k_{obs3}t} + b \quad (1)$$

where $k_{obs1}-k_{obs3}$ are the observed rate constants for the fast, intermediate, and slow phases, respectively, C_1-C_3 are the relative amplitude values for the three phases, and b is an offset value to account for a non-zero baseline. Observed rate constants for absorption changes occurring in the reductive half-reaction of Y259F DMGO with dimethylglycine were obtained from fits of the data to a standard double-exponential expression. In studies of the oxidative half-reaction, the enzyme was reduced anaerobically by titration with dithionite and rapidly mixed with a buffer containing a known concentration of dioxygen. Oxidative transients were analyzed using the appropriate rate expressions (see Results).

Crystallography. Crystals of the oxidized (resting) form of the H225Q mutant were obtained as described for the wild-type enzyme (*2*). Crystals were flash-cooled in liquid nitrogen, and diffraction data were collected at ID14 stations at ESRF (Grenoble, France). The oxidized "steady-state" structure was obtained by placing crystals of the oxidized form of the H225Q enzyme in a large volume of mother liquor supplemented with 100 mM dimethylglycine and flash-cooled after 1 min. No significant color change was observed during the soaking of these crystals. The substrate-reduced structure was obtained by soaking and flash-cooling crystals under conditions similar to those for the steady-state form, but using anaerobic conditions in a dedicated anaerobic glovebox. In this case, crystals rapidly turned colorless, indicating full reduction to the dihydroquinone.

Table 1: Data Collection and Final Refinement Statistics for the H225Q Mutant Crystal Structures

	resting state	steady state	substrate reduced
oxidation state[a]	oxidized	oxidized	reduced
space group	*C*222	*C*222	*C*222
resolution limits (Å)	20−1.30	20−2.0	20−1.9
no. of unique reflections	217590	57505	59254
I/σ_I	17.2	11.2	12.4
R_{merge} (%)	9.6	8.5	7.1
completeness	91.4	98.9	82.8
R/R_{free}	13.6/15.9	17.9/23.1	16.6/21.0
rmsd for bond lengths (Å)	0.010	0.021	0.015
rmsd for bond angles (deg)	1.372	1.764	1.536
average *B*-factor (Å^2)	13.0	27.1	14.7

[a] As estimated by visual inspection of crystals immediately prior to data collection.

Diffraction data were reduced and scaled using DENZO and SCALEPACK (*25*), and the structure was determined using difference Fourier methods. Atomic and *B* factor refinement for the individual structures was carried out using Refmac5 (*26*) alternated with manual rebuilding using Turbo-Frodo (*27*) and automated solvent model building using ArpWarp6.0 (*28*). An overview of diffraction data and final refinement and model statistics is given in Table 1.

RESULTS

Stopped-Flow Studies of Flavin Reduction in the H225Q Mutant of DMGO by Dimethylglycine. Spectral changes seen during the course of the reaction of H225Q DMGO with dimethylglycine were monitored using photodiode array spectroscopy (Figure 1). Time-dependent spectral changes were fitted globally by numerical integration methods using Prokin (Applied Photophysics Ltd.). The kinetic data were best fitted to a three-step model (A → B → C → D). Species A is the enzyme containing the FAD cofactor in the oxidized form. When species A converts to species B, there is a small degree of bleaching of flavin absorption (~20%), although the majority of the flavin remains in the oxidized form. A more substantial decrease in the absorbance at 444 nm occurs during the next phase (species B → species C), and the spectral changes that accompany formation of species C are indicative of flavin reduction. The spectrum of species C is typical of the dihydroflavin form of FAD. Species D accumulates at the end of the reductive half-reaction and has spectral properties very similar to those of species C, most noticeably that the flavin remains in the dihydroflavin form.

Single-wavelength stopped-flow absorption studies were performed with H225Q DMGO to investigate the substrate dependence of the individual phases seen in the diode array

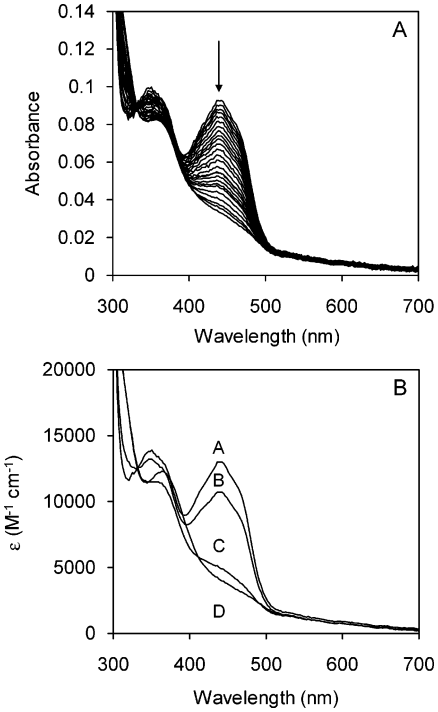

FIGURE 1: Reaction of H225Q DMGO with substrate monitored by stopped-flow photodiode array spectroscopy. (A) Time-dependent spectral changes on mixing H225Q DMGO with dimethylglycine (time base of 200 s). For clarity, only selected spectra are shown. (B) Deconvoluted spectra for the reaction shown in panel A. The data were fitted to a three-step model. The rate constants (inverse seconds) obtained from global fitting are 21.4 ± 0.08, 1.5 ± 0.004, and 0.28 ± 0.003 for the A → B, B → C, and C → D steps, respectively. Conditions: 10 mM sodium pyrophosphate buffer (pH 8.5) containing 20 μg/mL glucose oxidase and 11 mM glucose at 25 °C, 10 μM enzyme, and 50 mM substrate.

experiments. Consistent with the photodiode array data, transients at 444 nm were triphasic throughout the concentration range (Figure 2A). Analysis of the three kinetic steps as a function of dimethylglycine concentration also revealed that all three phases are dependent on substrate concentration (Figure 2B−D). Observed rate constants for the first, second, and third phases (k_{obs1}, k_{obs2}, and k_{obs3}, respectively) increase in a linear fashion as a function of substrate concentration with bimolecular rate constants (calculated from the slopes of the plots shown in Figure 2) of 0.26 ± 0.02 (first phase), 0.046 ± 0.001 (second phase), and 0.005 ± 0.0002 mM^{-1} s^{-1} (third phase). The linear plot for the first phase intercepts the ordinate axis with a value of 7.6 ± 2 s^{-1}. Given (i) the complexity of the reductive half-reaction in this mutant enzyme, (ii) the inference that this phase represents substrate C−H bond breakage (see below), and (iii) the proposed multiple conformational states for DMGO in single-turnover studies (see below), we are not able to comment at this stage on the mechanistic significance of this intercept value. Plots for the second and third phases intercept at zero on the ordinate.

With 50 mM protiated dimethylglycine at pH 8.5 and 25 °C, the observed rate constants calculated for the three phases of the reductive half-reaction of H225Q DMGO were 12, 1.5, and 0.25 s^{-1}, respectively, and 1, 0.14, and 0.03 s^{-1} for deuterated dimethylglycine. These results indicate that all three phases of flavin reduction in the H225Q mutant are isotope-sensitive (KIE ∼ 10), indicating that each phase is associated with breakage of the substrate C−H bond and FAD reduction.[2] In wild-type DMGO, it is the fast phase (limiting rate constant of 244 s^{-1}) only that is attributed to C−H bond breakage (*10*).

Steady-State Analysis of H225Q DMGO. We used the horseradish peroxidise-coupled enzyme assay to investigate the steady-state turnover behavior of H225Q DMGO. These assays revealed that the initial velocity was linearly dependent on DMG concentration across the experimental range (from 0 to 180 mM DMG). The value of k_{cat}/K_m determined from the slope of this plot is 0.06 ± 0.002 mM^{-1} s^{-1}. To calculate values for the true kinetic parameters K_m and k_{cat}, steady-state reactions of H225Q DMGO were performed using the enzyme-monitored turnover method, as performed previously for wild-type DMGO (*10*). A typical transient showing the time course for the absorption change (monitored at 444 nm) occurring during steady-state turnover for H225Q DMGO with DMG is shown in Figure 3A. At 444 nm, there is an initial rapid, but small (<10% of the total absorption change), decrease in the absorption, followed by the steady-state phase and then a final decrease as the fully reduced enzyme is formed because of depletion of molecular oxygen. The inset of Figure 3A shows the spectral forms of the H225Q mutant at different time points in the multiple-turnover analysis. Initially, the enzyme is in the oxidized form (point a on the trace) and remains largely in the oxidized form during the steady-state phase (point b on the trace). Following depletion of oxygen (point c on the trace), the enzyme is in the dihydroquinone form. Traces were collected at different concentrations of reducing substrate and analyzed as described previously (*24*). The traces represent a record of the rate of catalysis as a continuous function of oxygen concentration. Unlike the case for the wild-type enzyme which generates a series of lines that appear essentially parallel in a plot of the reciprocal of the turnover number versus the reciprocal of the oxygen concentration (*10*), a series of converging lines was obtained for the H225Q enzyme (Figure 3B). A secondary plot of the ordinate intercept versus dimethylglycine concentration is shown in Figure 3C, and a secondary plot of the slope versus dimethylglycine concentration is shown in Figure 3D. The true turnover number, k_{cat}, for the steady-state reaction is calculated from the ordinate intercept of this secondary plot (13.6 ± 1.9 s^{-1}), and the true K_m for dimethylglycine (142 ± 25 mM) is obtained by dividing the value of the gradient of this plot by the ordinate intercept. The true K_m for molecular oxygen (73 ± 17 μM) was obtained by multiplying the ordinate intercept of the secondary plot in Figure 3D by the true turnover number (13.6 s^{-1}). A comparison of the true kinetic parameters for the wild-type and H225Q enzyme is presented in Table 2.

Stopped-Flow Studies of Flavin Reduction in the Y259F Mutant of DMGO by Dimethylglycine. Multiple-wavelength stopped-flow spectroscopy was used to monitor the spectral changes that occur during the reductive half-reaction of Y259F DMGO with dimethylglycine (Figure 4). Data collected over a period of 500 s from the mixing event were best fitted to a two-step model (A → B → C). Species A

[2] The relatively high K_d for substrate and expense of deuterated DMG prevented detailed analysis of the effects of substrate concentration on each of the observed rate constants for FAD reduction.

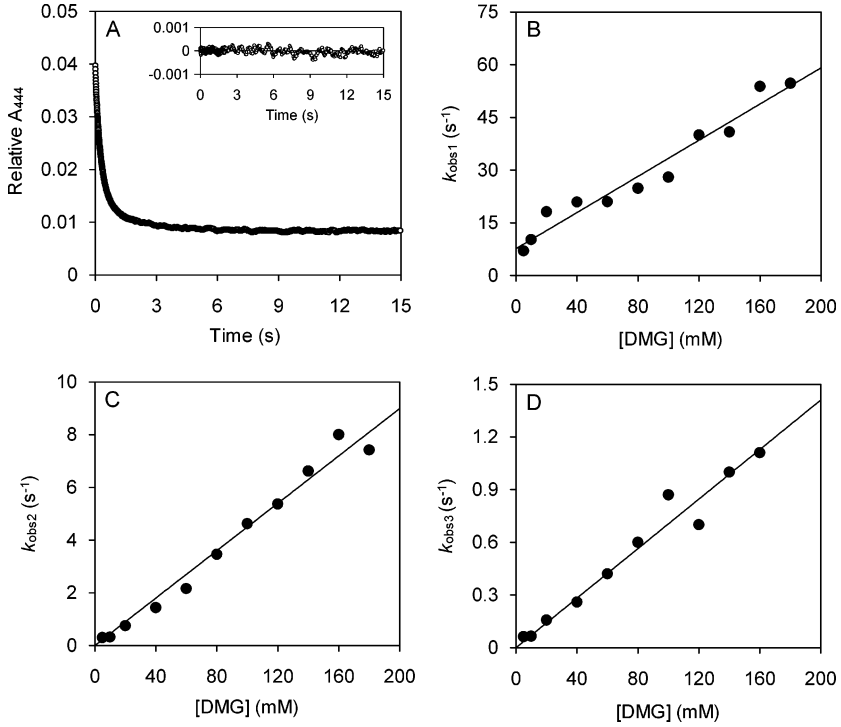

FIGURE 2: Kinetics of the reductive half-reaction of H225Q DMGO. (A) Triphasic absorption transient at 444 nm observed upon mixing of H225Q DMGO with DMG (80 mM). The inset is a plot of residuals from the fit to a triphasic rate expression. Concentration dependence of the rate for the fast phase [k_{obs1} (B)], the rate for the intermediate phase [k_{obs2} (C)], and the rate for the slow phase [k_{obs3} (D)] observed at 444 nm. Conditions: 10 mM sodium pyrophosphate buffer (pH 8.5) containing 20 μg/mL glucose oxidase and 11 mM glucose at 25 °C and 4 μM enzyme.

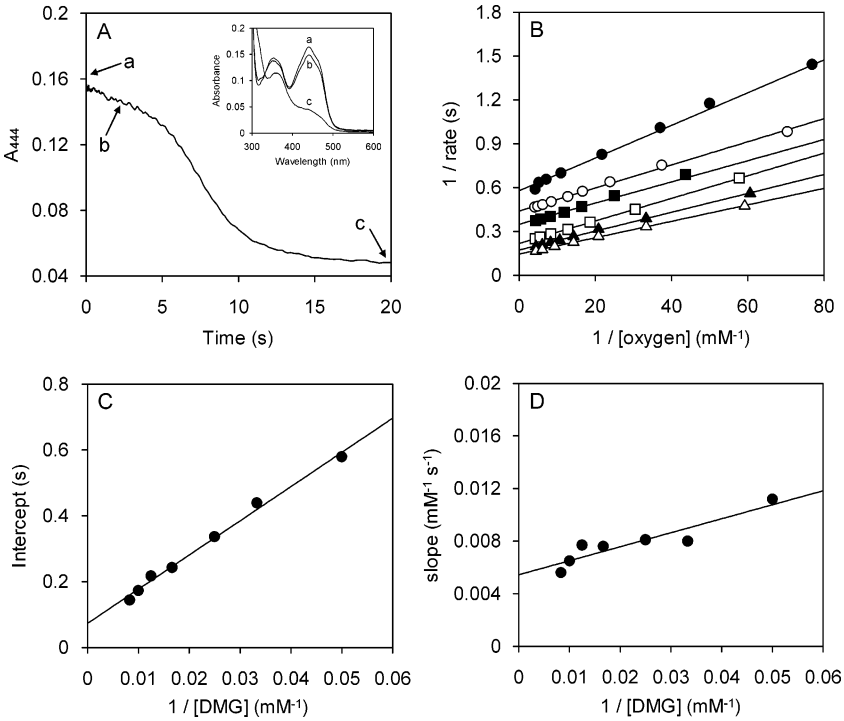

FIGURE 3: Enzyme-monitored turnover of H225Q DMGO in the stopped-flow instrument. (A) Enzyme (15 μM) reacted with 120 mM DMG in 10 mM sodium pyrophosphate buffer (pH 8.5) at 25 °C. The course of the reaction was monitored at 444 nm vs time. Arrow a shows the initial absorption, arrow b the steady-state phase, and arrow c the end of the reaction. The inset is the spectrum of the H225Q mutant recorded with a photodiode array detector at the indicated selected points in the time course of the main panel; the oxygen concentration was 0.258 mM. (B) Double-reciprocal plots of enzyme-monitored turnover data collected at various concentrations of DMG analyzed as described by Gibson et al. (*24*): (●) 20, (○) 30, (■) 40, (□) 80, (▲) 100, and (△) 120 mM DMG. For clarity, only selected lines on the reciprocal plot are shown. (C) A secondary plot of the ordinate intercepts of lines from the reciprocal plot (B) as a function of DMG concentration. (D) A secondary plot of the slopes of lines from the reciprocal plot (B) as a function of DMG concentration.

has spectral properties characteristic of the oxidized form of the enzyme (Figure 4B). Conversion of species A to species B is accompanied by bleaching of the enzyme-bound flavin and formation of the dihydroflavin form of FAD. A

Table 2: Kinetic Data Derived from Steady-State and Stopped-Flow Studies of Wild-Type and Mutant Forms of DMGO

	native DMGO	H225Q DMGO	Y259F DMGO
k_{lim} (flavin reduction)	244 s^{-1}	k_{obs1} = 0.26 mM^{-1} s^{-1} k_{obs2} = 0.046 mM^{-1} s^{-1} k_{obs3} = 0.005 mM^{-1} s^{-1}	0.16 s^{-1}
K_d[a] (mM)	~10	nd	60
K_m(DMG)[b] (mM)	2.4	142	47
K_m(O_2) (μM)	41	117	nd
k_{cat}[b] (s^{-1})	10.6	13.6	0.047

[a] The value given is the concentration of DMG required to give $0.5k_{lim}$. [b] Values for steady-state parameters were determined from a HRP assay for the Y259F enzyme; all other steady-state parameters were calculated from enzyme-monitored turnover experiments.

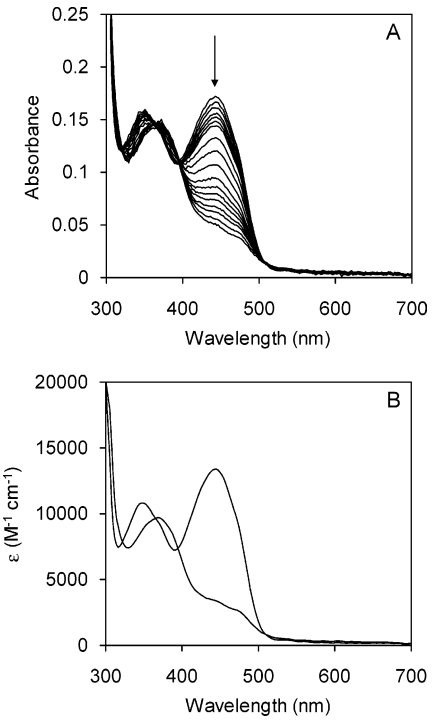

FIGURE 4: Reaction of Y259F DMGO with substrate monitored by stopped-flow photodiode array spectroscopy over a 200 s time base. Conditions: 10 mM sodium pyrophosphate buffer (pH 8.5) containing 20 μg/mL glucose oxidase and 11 mM glucose at 25 °C, 12 μM enzyme, and 50 mM substrate. (A) Time-dependent spectral changes upon mixing of Y259F DMGO with dimethylglycine. For clarity, only selected spectra are shown. (B) Deconvoluted spectra for the reaction shown in panel A. The data were fitted to a one-step model. The rate constant obtained from global fitting is 0.09 ± 0.01 s^{-1} for the A → B step.

small spectral change, resulting in further reduction of the enzyme, occurs during the final phase of the reaction (species B → C; not observed in Figure 4 where the time base is restricted to 200 s), but the flavin cofactor clearly remains in the dihydroflavin form. It should be emphasized that over the extended time base for FAD reduction in this mutant enzyme photoreduction of the FAD also becomes significant. Control experiments in which the Y259F enzyme was mixed with buffer alone indicated that FAD reduction by photoreduction becomes significant above 400 s. For this reason, it is not appropriate to attribute the spectral species observed in photodiode array spectroscopy to distinct enzyme species. Photoreduction, however, was not observed in single-wavelength acquisitions over 1000 s. In the single-wavelength mode, transients were biphasic. The concentration dependence of the two kinetic phases observed in the reductive half-reaction of Y259F DMGO was investigated in single-wavelength stopped-flow studies at 444 nm (Figure 5). The first kinetic phase, which contributes ~90% of the total signal change, exhibited a hyperbolic dependence on dimethylglycine concentration, and analysis using a hyperbolic equation (*29*) revealed that the limiting rate constant for flavin reduction (k_{lim}) was 0.16 ± 0.007 s^{-1} and the equilibrium dissociation constant for the oxidized Y259F DMGO−dimethylglycine complex was 60 ± 6.7 mM (Figure 5). The rate of FAD reduction is thus severely comprised [~1500-fold slower than that of the wild-type enzyme (Table 2)]. With 50 mM substrate, the kinetic isotope effect on FAD reduction is ~20, clearly indicating that breakage of the substrate C−H bond is rate-limiting for FAD reduction. The observed rate constant for the second kinetic phase was essentially independent of substrate concentration (k_{obs2} ~ 0.009 s^{-1}) in the pseudo-first-order regime (Figure 5). The small spectral change that accompanies the second phase in the Y259F enzyme occurs at a rate approximately 5-fold (0.009 s^{-1}) slower than the steady-state turnover number (0.047 s^{-1}; see below), and hence, we infer that this kinetic phase, the origin of which is unknown, is not relevant to steady-state catalysis.

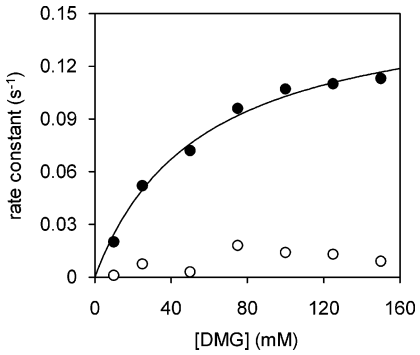

FIGURE 5: Concentration dependence of the kinetics of the reductive half-reaction of Y259F DMGO. Conditions: 10 mM sodium pyrophosphate buffer (pH 8.5) containing 20 g/mL glucose oxidase and 11 mM glucose at 25 °C and 5 μM enzyme. Concentration dependence of the rate for the fast phase [k_{obs1} (●)] and the rate for the slow phase [k_{obs2} (○)] observed at 444 nm.

Steady-State Analysis of Y259F DMGO. The horseradish peroxidase-linked assay yielded apparent k_{cat} and K_m values of 0.047 ± 0.001 s^{-1} and 47 ± 2.5 mM, respectively, for the Y259F mutant. The effect of the Tyr-259 → Phe substitution in DMGO is therefore an increase in the K_m for DMG by a factor of 14 and a decrease in the turnover number for the enzyme of ~200-fold when compared to those of the wild-type enzyme. Enzyme-monitored turnover studies of the Y259F mutant revealed that the absorption changes monitored at 444 nm were similar to those seen with the H225Q mutant. There is a small initial decrease in the absorption (~10% of the total absorption change), followed by a steady-state phase and then a final decrease in absorption due to exhaustion of molecular oxygen and formation of the fully reduced enzyme (Figure 6A). As observed with the H225Q mutant, it is the oxidized form of the Y259F mutant that accumulates during the steady-state phase of the reaction (see the inset of Figure 6A). Analysis of the kinetic data obtained with Y259F DMGO at different concentrations of

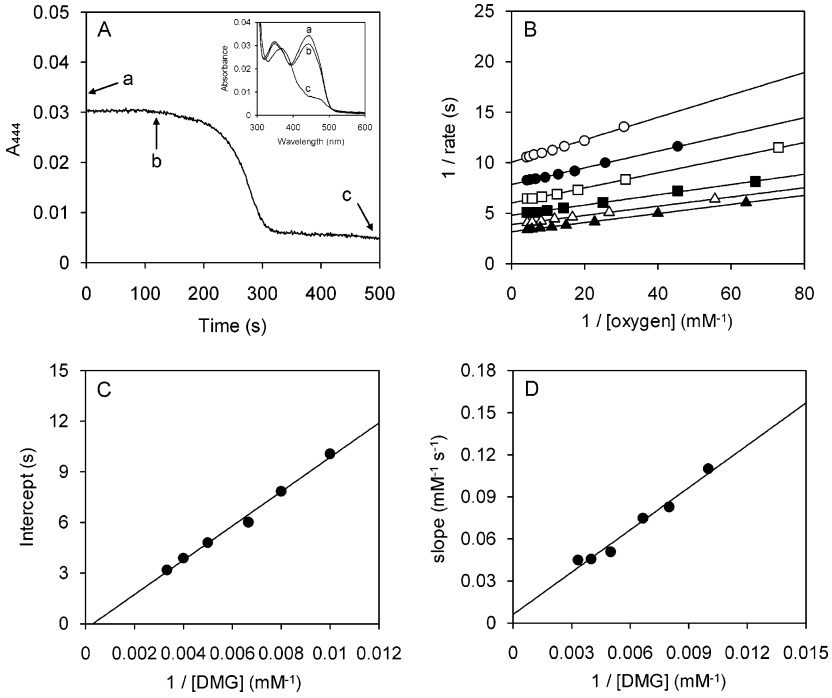

FIGURE 6: Enzyme-monitored turnover of Y259F DMGO in the stopped-flow instrument. (A) Enzyme (3 μM) reacted with 200 mM DMG in 10 mM sodium pyrophosphate buffer (pH 8.5) at 25 °C. The course of the reaction was monitored at 444 nm vs time. Arrow a shows the initial absorption, arrow b the steady-state phase, and arrow c the end of the reaction. The inset is the spectrum of the Y259F mutant recorded with a photodiode array detector at the indicated selected points in the time course of the main panel; the oxygen concentration was 0.258 mM. (B) Double-reciprocal plots of enzyme-monitored turnover data collected at various concentrations of DMG analyzed as described by Gibson et al. (*24*): (○) 100, (●) 125, (□) 150, (■) 200, (△) 250, and (▲) 300 mM DMG. (C) A secondary plot of the ordinate intercepts of lines from the reciprocal plot (B) as a function of DMG concentration. (D) A secondary plot of the slopes of lines from the reciprocal plot (B) as a function of DMG concentration.

reducing substrate showed that, unlike for the wild-type enzyme, plotting the reciprocal of the turnover number versus the reciprocal of the oxygen concentration produced a series of lines that were not parallel (Figure 6B). Secondary plots of the ordinate intercept versus dimethylglycine concentration and slope versus dimethylglycine concentration for the Y259F enzyme are shown in panels C and D of Figure 6, respectively. In general, the true turnover number, k_{cat}, for the steady-state reaction can be calculated from the ordinate intercepts of these secondary plots. However, for the steady-state reaction of Y259F DMGO, the plots intercept the ordinate axis very close to zero and have large errors associated with them, thus making it difficult to calculate, with confidence, a value for the turnover number for this mutant enzyme by this method.

Oxidative Half-Reaction Studies of DMGO Mutants. The oxidative half-reactions of the H225Q and Y259F mutant forms of DMGO were investigated under single-turnover, pseudo-first-order conditions, using enzymes reduced stoichiometrically with sodium dithionite. As observed with wild-type DMGO, re-oxidation of two-electron-reduced H225Q DMGO (monitored as an absorption change at 444 nm) occurs in a single kinetic process which is linearly dependent on oxygen concentration (Figure 7A). The rate constant for re-oxidation of dithionite-reduced H225Q DMGO is 240 ± 10 mM^{-1} s^{-1}, a value similar to that measured for the wild-type enzyme [342 mM^{-1} s^{-1} (*10*)]. The re-oxidation of dithionite-reduced Y259F DMGO by dioxygen was more complex and occurred in three phases (Figure 7B). However, the latter two phases made only small contributions to the total absorbance change (~10%). Each phase was linearly dependent on dioxygen concentration with rate constants of 270 ± 11, 60 ± 6, and 8 ± 2 mM^{-1} s^{-1}, respectively, for each of the three phases. Analysis of the oxidative half-reaction indicates that with both mutants the rate of FAD re-oxidation under standard aerobic conditions is faster than the rate of FAD reduction by substrate. This is consistent with enzyme-monitored turnover data which indicate that FAD reduction is rate-limiting in steady-state catalysis for both mutant enzymes.

Crystallographic Structure of the H225Q Enzyme. The oxidized H225Q structure was refined using data to 1.3 Å resolution. Significant changes in structure with the wild-type DMGO structure are limited to the immediate vicinity of the H225Q mutation. Like that of His-225 in the wild-type structure, the Gln-225 side chain is within hydrogen bonding of the Tyr-259 hydroxyl group (2.8 Å) (Figure 8A). Although the electron density indicates the amine group serves as a hydrogen bond acceptor for Tyr-259, a certain amount of disorder in the Gln-225 side chain position pre-empts strict determination of the exact amine side chain orientation, despite the high resolution obtained. The main conformation of the Gln-225 side chain is furthermore within hydrogen bonding distance of Tyr-272 (3.1 Å) which occupies two distinct positions, one of which allows for a (partially occupied) water molecule between Tyr-272 and Gln-225. The position of the Phe-335 and Phe-337 side chains resembles that of the wild-type structure in the absence of acetate with the Phe-335 phenyl group in close contact with the Gln-225 amine group. In contrast, the orientation of Tyr-259 is not affected by the H225Q substitution.

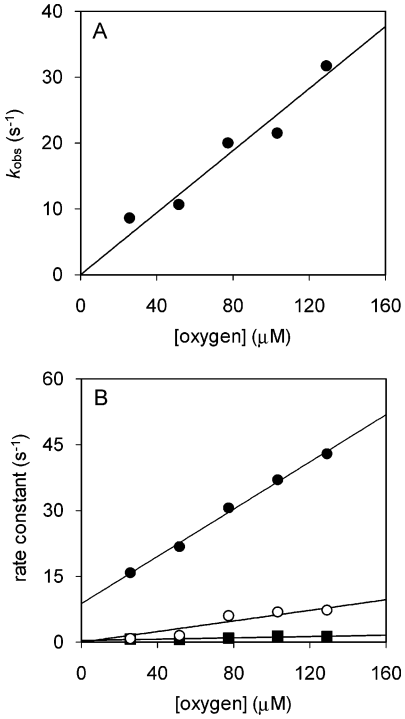

FIGURE 7: Kinetics of the oxidative half-reaction of H225Q and Y259F DMGO. Conditions: 10 mM sodium pyrophosphate buffer (pH 8.5) at 25 °C and 5 μM enzyme. (A) Plot of the observed rate of flavin oxidation vs oxygen concentration for dithionite-reduced H225Q DMGO. The bimolecular rate constant is 240 mM s^{-1}. (B) Plot of k_{obs1} (●), k_{obs2} (○), and k_{obs3} (■) vs oxygen concentration for the three phases of flavin oxidation for dithionite-reduced Y259F DMGO.

The structure of the H225Q mutant active site flash-cooled in a steady-state turnover situation was determined to 2.0 Å and is distinct from the resting-state structure (Figure 8B), although no electron density corresponding to substrate or product could be detected. The Gln-225 side chain is repositioned and forms a hydrogen bond with the oxygen backbone of Gln-226 (3.1 Å). This reorganization breaks the putative hydrogen bond with Tyr-259 and allows a (partially occupied) water molecule to be positioned close to N5 of the flavin and within hydrogen bonding distance of Gln-225, Tyr-259, and Tyr-272. Both the Phe-335 and Phe-337 phenyl group positions now resemble that of the wild-type DMGO−acetate complex (*2*; Figure 8C). In the H225Q mutant, this position is only possible with simultaneous repositioning of the Gln-225 side chain to avoid steric clash between Phe-335 and Gln-225 occupying the "resting-state" position. Substrate reduction of the H225Q mutant under anaerobic conditions followed by immediate flash-cooling reveals an active site structure that is very similar to the steady-state structure.

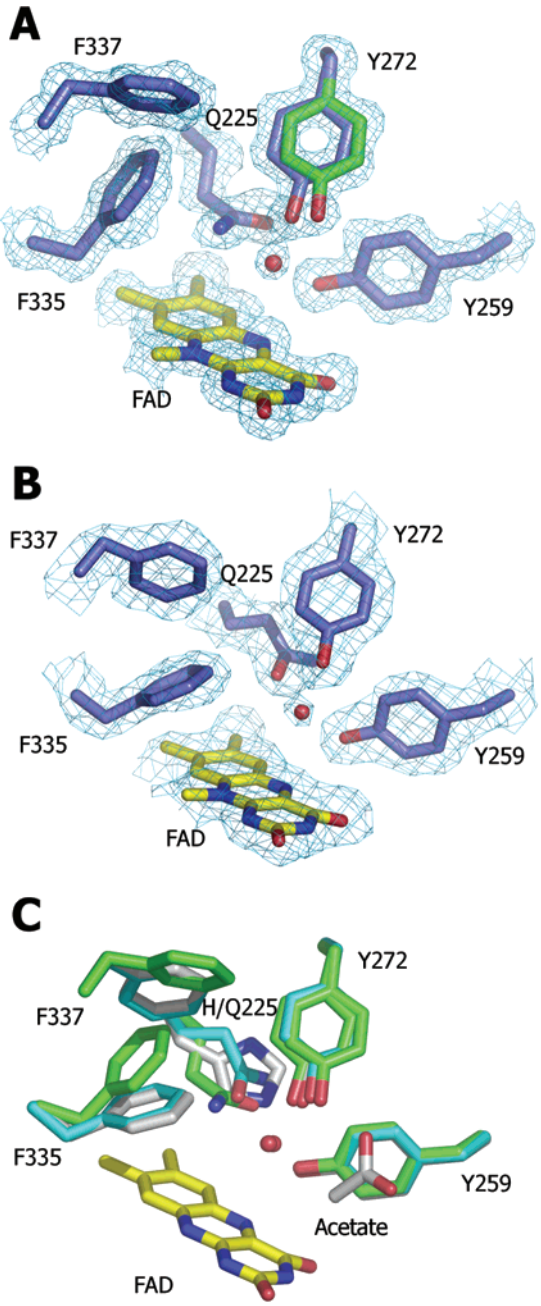

FIGURE 8: (A) Active site structure of the H225Q mutant in the resting state. The side chains of the key residues involved are shown as sticks with yellow carbons for the FAD isoalloxazine group and blue carbons for the protein. The minor conformation of Tyr-272 is shown with green carbons. The sigmaA-weighted $2F_o - F_c$ electron density is depicted at 1σ. (B) Active site structure of the H225Q mutant under steady-state conditions. Color coding and representation as in panel A. The sigmaA-weighted $2F_o - F_c$ electron density is depicted at 1σ. (C) Overlay of the different active site structures of the wild-type DMGO−acetate complex (gray carbons), the resting-state H225Q mutant (green carbons), and the steady-state H225Q mutant structure (cyan carbons).

DISCUSSION

His-225 and Tyr-259 of DMGO are two of only three active site residues (Gly-270 being the third residue) that are conserved throughout the family of SDH-like proteins (*2*). The roles of these residues in the structure and catalytic mechanism of DMGO have been probed by site-directed mutagenesis and the resulting mutants (H225Q and Y259F) studied by kinetic, spectroscopic, and crystallographic methods. Mutation of either residue occurs with the retention of catalytic activity, although the Y259F mutant is severely impaired in turnover and both mutants have elevated Michaelis constants for the substrate dimethylglycine (Table 2).

We have shown previously that FAD reduction in wild-type DMGO occurs in three distinct phases (*10*). The first phase involves reduction of the enzyme-bound flavin and displays a kinetic isotope effect of 2.9, consistent with substrate C−H bond cleavage. This phase is also dependent

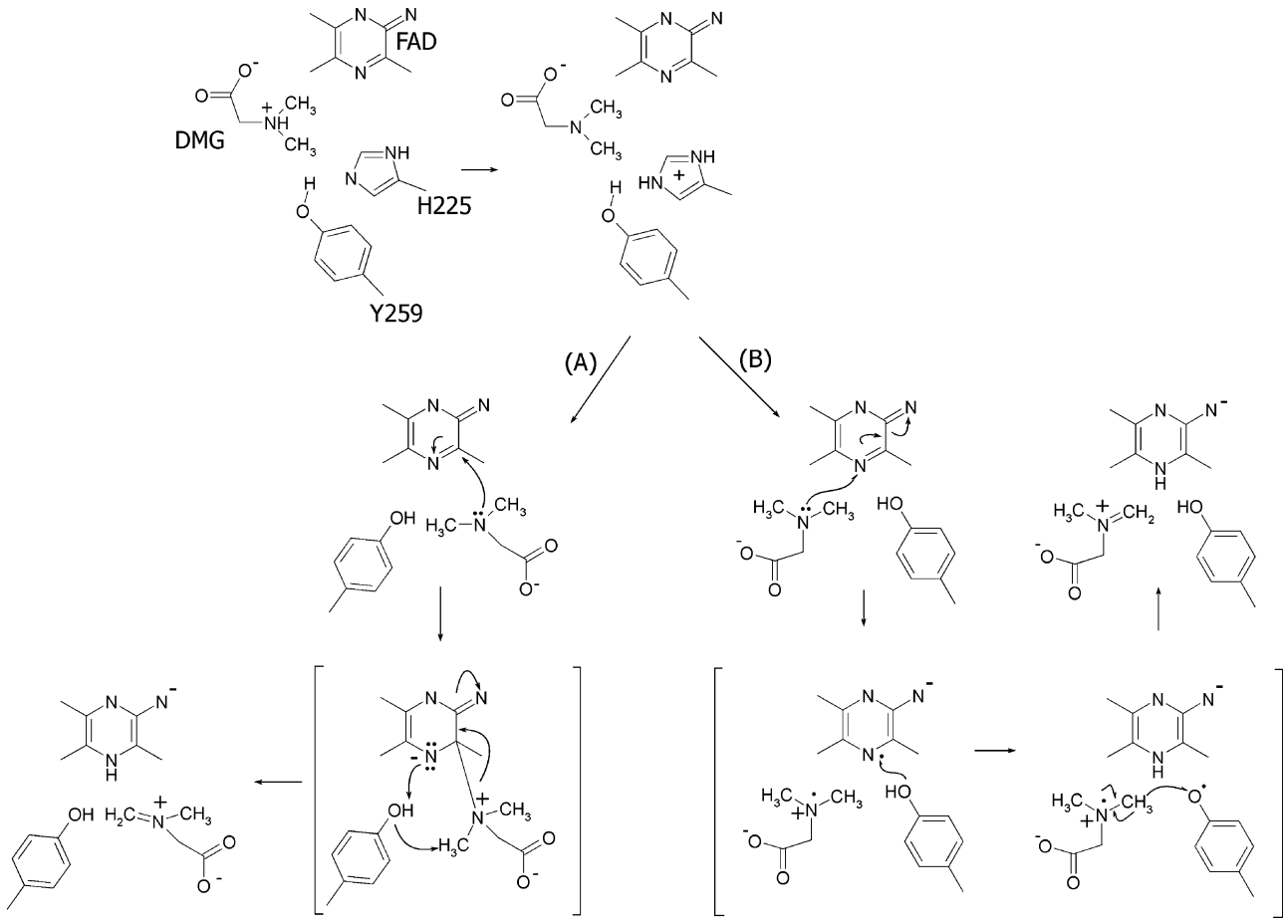

FIGURE 9: Proposed role of His-225 and Tyr-259 in the deprotonation of dimethylglycine in the dehydrogenase active site of DMGO. Following deprotonation of the substrate to generate the free base form, cleavage of the substrate C−H bond could occur either by the substrate−C4a adduct mechanism involving nucleophilic attack of the FAD by the unprotonated base (route A) or by the aminyl radical cation mechanism (route B).

on substrate concentration ($K_d \sim 10$ mM for the enzyme−dimethylglycine complex) and has a limiting rate constant for flavin reduction of 244 s^{-1}. Completion of this kinetic phase generates an intermediate with a broad spectral signature between 350 and 500 nm, which is attributed to a reduced enzyme−iminium charge-transfer species similar to those commonly seen during substrate oxidation in a number of flavoprotein oxidases. Decay of this intermediate (∼16 s^{-1}) is rate-limiting during steady-state turnover. The final phase (2 s^{-1}) is slower than the steady-state turnover rate (10.6 s^{-1}) and is therefore not relevant in steady-state catalysis. By contrast, we have shown that neither the Y259F nor the H225Q enzyme stabilizes the iminium−$FADH_2$ charge-transfer complex seen in stopped-flow studies of the wild-type enzyme (*10*) and that FAD reduction by substrate is rate-limiting during steady-state turnover (Figures 3A and 6A). The lack of a spectral signature for an iminium−$FADH_2$ charge-transfer species in the mutant enzymes suggests either (i) this charge-transfer species is not formed as a result of local structural perturbation in the active site following mutation or (ii) decay of this intermediate is faster than the preceding flavin reduction step.

Replacement of the imidazole side chain of His-225 with glutamine has removed the likely proton acceptor for Tyr-259. A water molecule resides close to Tyr-259 in some of the H225Q crystal structures and could serve as a putative proton acceptor. However, the position it occupies is mutually exclusive with the presumed location of the substrate [inferred on the basis of the wild-type DMGO−acetate complex (*2*)], making it highly unlikely that it is present in the enzyme−substrate complex. A requirement to displace this additional water molecule (absent in the wild-type enzyme) prior to substrate binding could provide some explanation for the significantly elevated K_m value obtained for the H225Q mutant (Table 2). The complex stopped-flow kinetic data obtained for the reduction of H225Q by substrate suggest the presence of distinct conformations with unique catalytic properties for the resting state of the enzyme. Indeed, the high-resolution crystal structure of the H225Q mutant reveals a certain amount of disorder in the position of Tyr-272 as well as Gln-225. In the wild-type enzyme, "closure" of the active site on binding acetate is accompanied by a repositioning of Phe-335 and Phe-337 (*2*), but these structural changes are incompatible with the main conformation of the Gln-225 side chain in the H225Q enzyme (Figure 8A). Surprisingly, crystal structures of the enzyme during steady-state turnover as well as the substrate-reduced enzyme reveal a conformational change that repositions Gln-225 in a manner that is concomitant with the repositioning of Phe-335 and Phe-337 to the closed state (Figure 8B).

Regardless of the observed conformational heterogeneity, both the kinetic and crystallographic results indicate His-225 does not play a crucial role in the catalytic mechanism. In contrast, the activity of theY259F enzyme is substantially,

Scheme 2

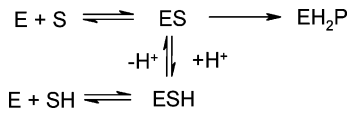

but not totally, impaired (Table 2). The observed data are compatible with the proposal that residues His-225 and Tyr-259 serve to deprotonate the substrate (*2*; Figure 9 and Scheme 2). Specifically, Tyr-259 acts as an active site base, and its acid−base properties are likely modulated by its close interaction with His-225. In the case of the H225Q mutant, we suggest deprotonation of Tyr-259 (by solvent) occurs at a more elevated pH than in the wild-type enzyme, the latter deprotonation being assisted by the presence of His-225.[3] In this case, it is possible that the conformational heterogeneity observed for the resting-state structure of H225Q DMGO in the vicinity of Tyr-259 influences the pK_a of this residue, thus affecting the individual catalytic properties of the distinct conformations. This is consistent with the observed complexity of the stopped-flow transients for the H225Q enzyme. In the case of the Y259F mutant, the remaining activity could be a consequence of binding a small amount of deprotonated (reactive) substrate. The amount of free amine substrate available in solution at pH 8.5 is relatively small given the high pK_a (9.89) of dimethylglycine. This situation would give rise to an elevated apparent dissociation constant for substrate (substrate concentration measured as the sum of the concentrations of the protonated amine cation and the free base form) and a diminished rate constant for FAD reduction (since the enzyme is not saturated with unprotonated substrate). In the wild-type enzyme, the His-225 and Tyr-259 residues are able to assist the reaction by deprotonating the substrate when bound as part of the Michaelis complex.

Other amine oxidases have been shown to preferentially bind and react with the deprotonated substrate (*30*, *31*). We suggest that in DMGO the His-Tyr pair ensures that the unprotonated form of the substrate is present in the active site before FAD reduction (Figure 9). Thus, the role of Tyr-259 is to prime the substrate for reaction by deprotonating the amine group prior to FAD reduction. During the FAD reduction step, the precise mechanism of C−H bond cleavage remains to be determined but in principle could involve either (i) formation of an aminium radical cation species [akin to a proposed mechanism for monoamine oxidase (*18*, *19*)] or (ii) a mechanism involving nucleophilic attack at the FAD C4a position (Figure 9), also proposed for monoamine oxidase (*22*) and trimethylamine dehydrogenase (*23*). We should emphasize, however, that no tyrosyl radical species has been observed in DMGO, and such a species would be required to support an aminium radical cation mechanism. Moreover, if such a species were to exist (which would be presumed to form on Tyr-259), the residual activity seen in the Y259F enzyme mutant would only be explained by assuming that alternative residues close to the flavin also function as alternative electron donors to the FAD semiquinone species. In the alternative C4a nucleophilic attack mechanism, the role of Tyr-259 is to deprotonate the substrate amine cation prior to covalent addition to the FAD C4a position. The residue could also assist in H-transfer between N5 and the substrate methyl group (Figure 9). In this case, the small amount of substrate-free base that is also present in solution could account for the residual activity found in the Y259F mutant.

Concluding Remarks. Our kinetic and crystallographic data for the H225Q and Y259F DMGO enzymes are consistent with the need to deprotonate the substrate cation prior to reduction of the FAD during oxidation of dimethylglycine. We suggest that Tyr-259 is the active site base in the wild-type enzyme responsible for deprotonating the substrate, thus accounting for the substantial loss of activity in the Y259F mutant. The acid−base properties of Tyr-259 are likely to be influenced by the interaction of this residue with His-225, as observed in the structure of wild-type DMGO. Following deprotonation of the substrate, and as with other flavin-dependent oxidases/dehydrogenases, the precise mechanism of substrate C−H bond cleavage remains uncertain. Our data are consistent with contemporary mechanisms in the field involving either radical cleavage of the substrate C−H bond (the aminyl radical cation mechanism) or a proton abstraction mechanism from a C4a−substrate adduct.

[3] Compared to that of the wild-type enzyme, the relatively small yields of the Y259F enzyme have prevented us from performing a rigorous pH dependence study of the rate of FAD reduction and thus detailed analysis of the kinetically defined macroscopic pK_a values for this reaction. Likewise, the complexity of the reductive half-reaction for the H225Q enzyme attributed to the multiple conformational states of the mutant has prevented us from analyzing the pH dependence of FAD reduction in this mutant enzyme.

REFERENCES

1. Meskys, R., Harris, R. J., Casaite, V., Basran, J., and Scrutton, N. S. (2001) Organization of the genes involved in dimethylglycine and sarcosine degradation in *Arthrobacter sp.*: Implications for glycine betaine catabolism, *Eur. J. Biochem. 268*, 3390−3398.
2. Leys, D., Basran, J., and Scrutton, N. S. (2003) Channelling and formation of 'active formaldehyde' in dimethylglycine oxidase, *EMBO J. 22*, 4038−4048.
3. Trickey, P., Wagner, M. A., Jorns, M. S., and Mathews, F. S. (1999) Monomeric sarcosine oxidase: Structure of a covalently flavinylated amine oxidizing enzyme, *Struct. Folding Des. 7*, 331−345.
4. Binda, C., Coda, A., Angelini, R., Federico, R., Ascenzi, P., and Mattevi, A. (1999) A 30-angstrom-long U-shaped catalytic tunnel in the crystal structure of polyamine oxidase, *Struct. Folding Des. 7*, 265−276.
5. Schreuder, H. A., Mattevi, A., Obmolova, G., Kalk, K. H., Hol, W. G., van der Bolt, F. J., and van Berkel, W. J. (1994) Crystal structures of wild-type *p*-hydroxybenzoate hydroxylase complexed with 4-aminobenzoate, 2,4-dihydroxybenzoate, and 2-hydroxy-4-aminobenzoate and of the Tyr222Ala mutant complexed with 2-hydroxy-4-aminobenzoate. Evidence for a proton channel and a new binding mode of the flavin ring, *Biochemistry 33*, 10161−10170.
6. Lee, H. H., Kim, D. J., Ahn, H. J., Ha, J. Y., and Suh, S. W. (2004) Crystal structure of T-protein of the glycine cleavage system. Cofactor binding, insights into H-protein recognition, and molecular basis for understanding nonketotic hyperglycinemia, *J. Biol. Chem. 279*, 50514−50523.
7. Teplyakov, A., Obmolova, G., Sarikaya, E., Pullalarevu, S., Krajewski, W., Galkin, A., Howard, A. J., Herzberg, O., and Gilliland, G. L. (2004) Crystal structure of the YgfZ protein from *Escherichia coli* suggests a folate-dependent regulatory role in one-carbon metabolism, *J. Bacteriol. 186*, 7134−7140.
8. Scrima, A., Vetter, I. R., Armengod, M. E., and Wittinghofer, A. (2005) The structure of the TrmE GTP-binding protein and its implications for tRNA modification, *EMBO J. 24*, 23−33.
9. Scrutton, N. S., and Leys, D. (2005) Crystal structure of DMGO provides a prototype for a new tetrahydrofolate-binding fold, *Biochem. Soc. Trans. 33*, 776−779.
10. Basran, J., Bhanji, N., Basran, A., Mistry, S., Meskys, R., and Scrutton, N. S. (2002) Mechanistic aspects of the covalent

flavoprotein dimethylglycine oxidase of *Arthrobacter globiformis* studied by stopped-flow spectrophotometry, *Biochemistry 41*, 4733−4743.
11. Kubo, H., Watari, H., and Shiga, T. (1959) Study on an intermediate form in the oxidation-reduction of D-amino acid oxidase, *Bull. Soc. Chim. Biol. 41*, 981−988.
12. Massey, V., and Gibson, Q. H. (1964) Role of semiquinones in flavoprotein catalysis, *Fed. Proc. 23*, 18−29.
13. Yagi, K., Okamura, K., Naoi, M., Sugiura, N., and Kotaki, A. (1967) Mechanism of enzyme action. II. Characterization of the purple intermediate in the anaerobic reaction of D-amino-acid oxidase with D-alanine, *Biochim. Biophys. Acta 146*, 77−90.
14. Kumagai, H., Yamada, H., Suzuki, H., and Ogura, Y. (1971) Action mechanism of tyramine oxidase from *Sarcina lutea*, *J. Biochem. 69*, 137−144.
15. Koyama, H., and Suzuki, H. (1986) Spectral and kinetic studies on *Pseudomonas* L-phenylalanine oxidase (deaminating and decarboxylating), *J. Biochem. 100*, 859−866.
16. Scrutton, N. S. (2004) Chemical aspects of amine oxidation by flavoprotein enzymes, *Nat. Prod. Rep. 21*, 722−730.
17. Rohlfs, R. J., and Hille, R. (1994) The reaction of trimethylamine dehydrogenase with diethylmethylamine, *J. Biol. Chem. 269*, 30869−30879.
18. Rigby, S. E. J., Hynson, R. M. G., Ramsay, R. R., Munro, A. W., and Scrutton, N. S. (2005) A stable tyrosyl radical in monoamine oxidase A, *J. Biol. Chem. 280*, 4627−4631.
19. Silverman, R. B. (1995) Radical thoughts about the life of MAO, *Prog. Brain Res. 106*, 23−31.
20. Edmondson, D. E. (1995) Aminium cation radical mechanism proposed for monoamine oxidase B catalysis: Are there alternatives? *Xenobiotica 25*, 735−753.
21. Kim, J., Bogdan, M., and Mariano, P. S. (1993) Mechanistic analysis of the 3-methyllumiflavin-promoted oxidative deamination of benzylamine. A potential model for monoamine oxidase catalysis, *J. Am. Chem. Soc. 115*, 10591−10595.
22. Miller, J. R., and Edmondson, D. E. (1999) Structure-activity relationships in the oxidation of para-substituted benzylamine analogues by recombinant human liver monoamine oxidase A, *Biochemistry 38*, 13670−13683.
23. Basran, J., Sutcliffe, M. J., and Scrutton, N. S. (2001) Deuterium isotope effects during C-H bond cleavage by trimethylamine dehydrogenase: Implications for mechanism and vibrationally assisted H-tunneling in wild-type and mutant enzymes, *J. Biol. Chem. 276*, 24581−24587.
24. Gibson, Q. H., Swoboda, B. E. P., and Massey, V. (1964) Kinetics and mechanism of action of glucose oxidase, *J. Biol. Chem. 239*, 3927−3934.
25. Otwinowski, Z., and Minor, W. (1997) Processing of X-ray diffraction data collected in oscillation mode, *Methods Enzymol. 279*, 307−326.
26. Murshudov, G. N., Vagin, A. A., and Dodson, E. J. (1997) Refinement of macromolecular structures by the maximum-likelihood method, *Acta Crystallogr. D53*, 240−255.
27. Roussel, A., and Cambillau, C. (1992) *TURBO-FRODO*, Biographics, architecture and fonction des macromolecules biologiques (AFMB), Marseilles, France.
28. Perrakis, A., Morris, R., and Lamzin, V. S. (1999) Automated protein model building combined with iterative structure refinement, *Nat. Struct. Biol. 6*, 458−463.
29. Strickland, S., Palmer, G., and Massey, V. (1975) Determination of dissociation constants and specific rate constants of enzyme-substrate (or protein-ligand) interactions from rapid reaction kinetic data, *J. Biol. Chem. 250*, 4048−4052.
30. Basran, J., Sutcliffe, M. J., and Scrutton, N. S. (2001) Optimising the Michaelis complex of trimethylamine dehydrogenase: Identification of interactions that perturb the ionisation of substrate and facilitate catalysis with trimethylamine base, *J. Biol. Chem. 276*, 42887−42892.
31. Zhao, G., and Jorns, S. (2002) Monomeric sarcosine oxidase: Evidence for an ionizable group in the E•S complex, *Biochemistry 41*, 9747−9750.

BI061094D